THE DISTRIBUTION OF 20-900M CRATERS IN THE LUNAR POLAR REGIONS. E. Mazarico[1], P. Pokorny[2,1], P. Mahanti[3], J.-P. Williams[4], C. Fassett[5], M. Kinczyk[5], M.S. Robinson[3]. [1]NASA Goddard Space Flight Center, 8800 Greenbelt Road, Greenbelt, Maryland, USA (erwan.m.mazarico@nasa.gov). [2]Catholic University of America, Washington, DC, USA. [3]Intuitive Machines, Inc., Phoenix, Arizona, USA. [4]University of California, Los Angeles, California, USA. [5]Johns Hopkins University, Applied Physics Laboratory, Laurel, Maryland, USA.

Introduction: The mapping and analysis of the distribution of impact craters on planetary surfaces is a critical method for understanding the geologic history of planetary bodies. The largest impacts define major geologic ages, but these larger events are not as relevant to recent history because they are now exceedingly rare. The smallest impacts, in contrast, with their short crater degradation lifetime, inform recent geologic events. But their extremely large number has so far prevented their exhaustive mapping and analysis. These small crater populations inform questions such as the effects of target properties [1] and permanent shadow [2] on crater retention. Here, we use the images of polar shadow acquired by the NASA ShadowCam instrument [2] onboard the Korea Pathfinder Lunar Orbiter (KPLO) to investigate the spatial distribution of small craters (<1 km), including areas in permanent shadow. This abstract focuses on the southern polar region, but ShadowCam has to date mapped significant portions of both polar regions in both summer and winter seasons in 2023/2024.

Crater Detection from ShadowCam Images: Machine learning techniques enable large image datasets to be analyzed quickly, particularly useful for traditionally time-consuming tasks such as feature detection [3,4]. Automated crater detection is particularly well-adapted to small craters, as they are typically symmetric. As explained in detail in the companion abstract [5], we used a neural network based on the YOLOv8 architecture for feature detection. We started with the training data used to identify small craters in LROC-NAC images [6], to which we added about 50,000 craters, first detected from ShadowCam images and then manually validated. This updated neural network was then applied to the 13,121 full-resolution ShadowCam images, available on the PDS. For each image, we obtain a list of georeferenced bounding boxes encompassing the detected crater and a corresponding image mask (sampled, unsaturated pixels). Crater diameters are computed from the size of the detection bounding boxes, which may currently be slight overestimates. Crater degradation state is also not observed and considered at this time. In total, more than 1 billion craters were detected. However, there is significant overlap and repeat coverage in the ShadowCam image dataset, so most of these detections are duplicates.

Crater Spatial Density Mapping: Because the geolocation accuracy of the images is on a par with the size of the smallest detected craters (~20 m), it is difficult to obtain a combined crater catalog for each polar region. Instead, we first created, for each image, a set of 18 spatial density maps of craters over fixed diameter bins, logarithmically covering the 14-900 m range (14 to 17.6 m, 17.6 to 22.2 m, etc.). The resolution of these maps is 100 m/pixel. Because the geolocation accuracy level is better, it allows combining density maps from individual images with negligible smearing. For each crater diameter bin, all the spatial density maps are combined into a single map covering each 80°-90° polar region, minimizing coverage gaps and lighting biases present in single images. Figure 1 shows one of these maps for the south polar region. Based on these, our current total number of unique mapped craters in the southern polar region is ~32.9 million.

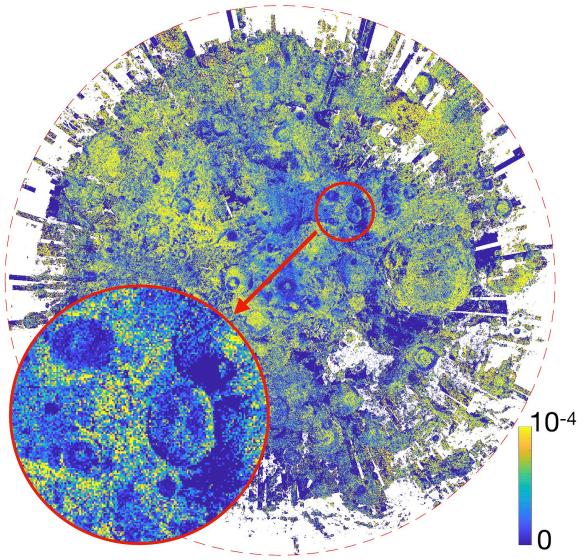

Figure 1. Map of spatial density of the 17.6-22.2 m diameter craters in the 80-90°S region. The colorscale is `parula` between 0 and 10^{-4} m^{-2}.

With these two sets of 18 regional crater spatial density maps in hand, we can compute the crater size-frequency distribution, either of the whole region or of subregions.

Preliminary Crater Density Trends: This comprehensive mapping of the small-crater population allows us to study how the crater size-frequency distribution (CSFD) varies spatially, due to other terrain characteristics. We first look at how slope affects the CSFD. We use the LOLA 100m-baseline slope map [7], to define eight spatial subsets, one for each 5° slope bin in order to span the 0-40° range. We then compute each CSFD using only the appropriate 100 m pixels. Figure

2 shows the eight computed CSFDs, and with the corresponding "R-plots" (CSFD spectrum rectified by D^3). A clear trend appears, with lower slopes retaining more small craters than higher slopes. While previously recognized over small regions [8], we can quantitatively confirm this result over a large region (80-90°S) and for crater sizes down to ~18 m diameter. (Note that the very first bin does not follow the trend, indicating the completeness limit is ≲18 m). The apparent relative paucity of 200-500 m craters for slopes >20°, which may be due to the choice of the slope baseline (100 m), will be investigated further.

We also computed the CSFD of the permanently and non-permanently shadowed terrains, and we find that the PSR CSFD lies above the non-PSR CSFD (not shown). However, in the 80-90°S study region, the PSR terrain does not follow the overall slope distribution, so we instead repeat the slope-trend analysis described above for both PSR and non-PSR terrain types (Figure 3). We find that, at comparable slopes, the PSR terrain appears to be slightly less cratered than non-PSR terrain. The log-log trend of the PSR CSFDs is less uniform than for the non-PSR terrain, and needs further investigation.

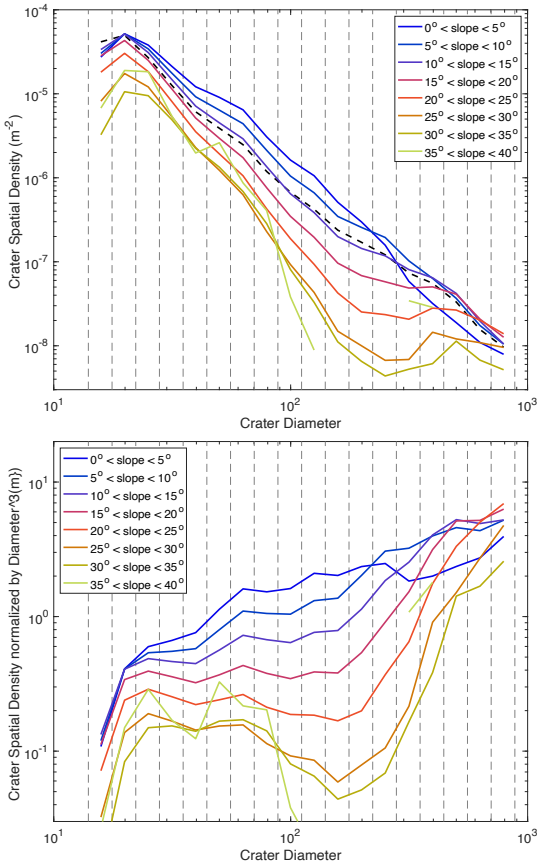

Figure 2. (top) CSFD over the lunar south polar region (80-90°S) computed for a series of terrain slopes (0-40°). The whole-region CSFD is shown as dashed black. (bottom) Corresponding R-plots.

Future Work: We will continue improving the crater spatial density maps by adding more recent ShadowCam images, investigate the effect of slope baseline on the CSFDs and their interpretation. We will consider other trends, *e.g.*, vs. temperature or geological unit. We will extend the study to the north pole, increasing the sampled area and allowing inter-comparison.

Acknowledgements: We thank the KPLO and ShadowCam operations and science teams for acquiring the ShadowCam dataset. PP was supported by the NASA Planetary Science Division Research Program through the GSFC Planetary Geodesy ISFM.

References: [1] J.-P. Williams *et al.*, AGU 2024; [2] M.S. Robinson *et al.*, 2023, *J. Astron. Space Sci.*, 10.5140/JASS.2023.40.4.149; [3] V. Bickel *et al.*, 2022, *GRL*, 10.1029/2022GL098812 ; [4] O. Rüsch *et al.*, 2023, *PSJ*, 10.3847/PSJ/acd1ef ; [5] P. Pokorny *et al.*, LPSC 2025; [6] Fairweather et al., 2023, *ESS*, 10.1029/2021EA002177 ; [7] M.K. Barker *et al.*, 2023, *PSJ*, 10.3847/PSJ/acf3e1; [8] A.T. Basilevsky et al., LPSC 1976.

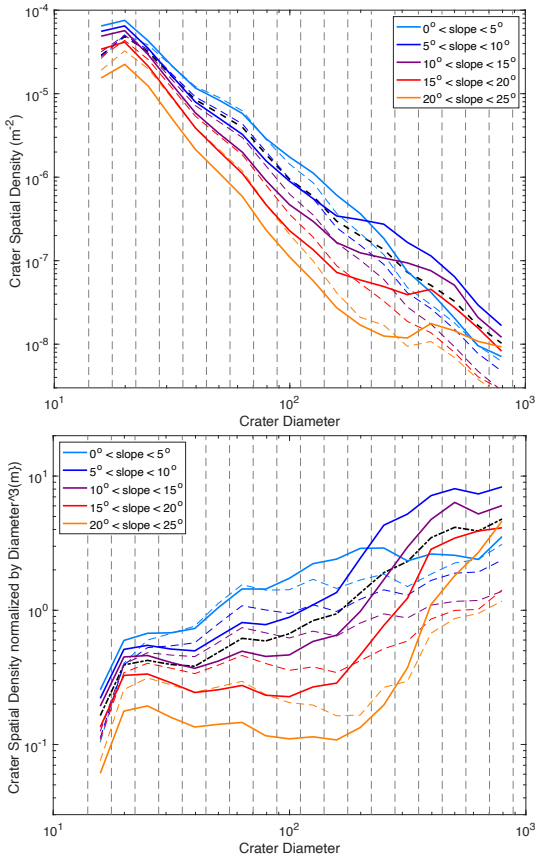

Figure 3. (top) Crater Size Frequency Distribution over the lunar south polar region (80-90°S) computed for each illumination terrain type (solid: PSR; dashed: not PSR) over a series of terrain slopes (0-40°). The whole-region CSFD is shown as dashed black. (bottom) Corresponding R-plots.